Multimedia Tools and Applications (2020) 79:26123–26138
https://doi.org/10.1007/s11042-020-09159-z

Disparity-preserving image rectangularization for stereoscopic panorama

I-Cheng Yeh[1] · Shih-Syun Lin[2] · Shuo-Tse Hung[3] · Tong-Yee Lee[4]

Received: 10 August 2019 / Revised: 28 May 2020 / Accepted: 4 June 2020 /
Published online: 10 July 2020

Abstract
This study aims at generating a long strip stereoscopic panorama with a rectangular boundary from a stereoscopic video. The issues arising from this goal are how to automatically select appropriate frames to reduce geometric distortion in image stitching, how to preserve disparity under image warping, and how to generate a rectangular panoramic stereoscopic image without the loss of boundary information. To deal with these issues and to generate visually smooth stereoscopic panorama, a disparity-aware image warping is proposed. Moreover, the image warping method is performed on the irregular left and right panoramic images simultaneously with a hybrid control mesh to generate a rectangular panorama while preserving the spatial shape and disparity as much as possible. Experimental results on various stereo video contents show that the proposed method can effectively preserve both the spatial shapes and pixel disparity.

Keywords Video processing · Stereoscopic panorama · Image warping · Disparity preserving

✉ Tong-Yee Lee
tonylee@mail.ncku.edu.tw

I-Cheng Yeh
ichenyeh@saturn.yzu.edu.tw

Shih-Syun Lin
linss@mail.ntou.edu.tw

Shuo-Tse Hung
hungshoutse@gmail.com

[1] Yuan Ze University, Taoyuan City, Taiwan

[2] National Taiwan Ocean University, Keelung City, Taiwan

[3] MStar Semiconductor, Inc., Hsinchu, Taiwan

[4] National Cheng-Kung University, Tainan City, Taiwan

1 Introduction

With the development of digital photography and video recording, an increasing number of video clips has been produced. Using a wide-angle view to overview a large outdoor scene is a common technique in natural landscape photography. However, due to the acquisition limitation of imaging equipment, it is difficult to capture a wide-angle view in a single camera shot. Therefore, a number of researches on wide-angle view generation has been proposed. Although traditional 2D image stitching from a set of image or video frames has been extensively studied [30] and [31], the stereoscopic wide-angle view synthesis is still a challenging task.

The term "panorama" originally appeared in the 18^{th} century, used by the Irish painter Robert Barker to describe his painting shown in Fig. 1. The concept of panorama was first derived from large-scale mural and spherical dome paintings. Most painted panoramas serve to present a wide-angle, a landscape view, or a series of narrative illustrations.The existing panoramas can be classified into two categories, *360-degree panorama* and *rectangular panorama*, based on the panorama shape, a *360-degree panorama* shows a complete view of the surrounding environment, which is typically constructed from a series of input images that have been captured from a common viewpoint. Most of these panoramas are used to present a series of stories in a static scene, displayed in religious and historical buildings. Another category is *rectangular panorama* in which the panorama is constructed from a series of images taken by a panning shot in an outdoor scene and generally has a rectangular boundary to fit a common display device or printing purpose. These kind of panoramas may contain more possibility for the illustration of a landscape scene and the contents of a video overview. In this paper, we focus on rectangular panoramic images under the assumption that input stereo videos are acquired from a panning stereoscopic video camera. Instead of using a sequence of crafted stereoscopic images in panorama generation, the proposed method automatically extracts representative frames from a stereoscopic video to maximize image quality and conveying spatiotemporal information presented in input videos. In the meantime, the distortion of pixel disparity and object shapes have to be minimized simultaneously. Therefore, the disparity-aware control and shape-preserving warping in previous work [16] are adopted to align the features in the left eye view and right eye view while the depth information in stereoscopic panoramas is maintained.

2 Related work

Recent and related studies on panorama images are reviewed only in this section. For the history of panorama techniques, readers can refer to Oettermann et al. [21]. Shum et al. [24] present a system to construct a panoramic image by mosaicking a sequences of images.

Fig. 1 Panorama of London by Robert Barker, 1792

Finding suitable source images to generate panorama is a challenging task; hence, Liu et al. [19] design a system to generate a panorama from casually shot videos. To incorporate dynamics of input video, Agarwala et al. [1] propose a method to stitch a panoramic video texture which can be played indefinitely as a dynamic background. Along with the plethora of panorama techniques, many methods on seamless image stitching have been proposed. Brown et al. [4] formulate stitching as a multi-image matching problem and utilize invariant local features to find matches. Other recent works focus on handling parallax problems. Zhang et al. [31] tackle the parallax problem by adapting a hybrid alignment model that combines homography and content-preserving warping to provide flexibility for parallax and object distortion avoidance. In this study, we generate a rectangular panoramic image which is stitched from frames of an input stereoscopic video. The naïve cropping on image boundary has been proved inappropriate in boundary rectangularizing because of the loss of regional information and the reduction of the viewing frustum angle. Therefore, He et al. [13] adopt a seam carving technique to re-fill irregular boundaries and establish correspondence between the irregular panorama and a desired rectangular shape. By contrast, a content-aware warping is proposed to generate a rectangular panorama. Moreover, to adapt the irregularity of stitched panorama and to preserve shape-context features, a hybrid mesh that combines a general quad-based mesh with a triangle-based boundary strip [23, 25] is used. In addition, Barnes et al. [2] and Kopf et al. [15] propose using image completion techniques in irregular panorama rectangularizing. These two works have similar advantages and disadvantages coming from image completion. They may fail at the boundary of a complicated scene that contains non-repetitive object information.

Along with the rapid growth of 3D cinema, tremendous effort has been devoted to stereoscopic data processing. The quality of visual perception on depth is important in stereoscopic data. Hence, recent researches address how to handle depth information along with image quality. Chang et al. [8] propose a content-aware stereoscopic image display adaptation method that fits different sizes while preserving object shapes and adjusting suitable depth information. Since applying image warping on stereoscopic images may change disparity information unpredictably, Niu et al. [20] present a framework to extend traditional image warping technique to handle stereoscopic images. Lin et al. [17] consistently adapt a stereoscopic image to fit various aspect ratios while preserving salient contents. The approach in [27] is another type of stereoscopic image editing, which addresses seamless stereoscopic image stitching. By contrast, this study focuses on stereoscopic image rectangularizing and spatial and stereo object preservation.

3 Methodology

The proposed system consists of three main steps, *representative frame selection*, *image stitching*, and *boundary rectangularizing* as shown in Fig. 2. In the first step, the system selects a series of representative frames uniformly that can effectively represent the input video. Then, the selected frames are stitched into an irregular panoramic image in the second step and generate a rectangular panorama in the third step. Meanwhile, to provide correct depth perception, we align features of the left and right panoramic images separately. These steps are described in the following subsections.

3.1 Representative frame selection and image stitching

Utilizing all video frames in image stitching is redundant and unnecessary.In general, the representative frames are selected based on three aspects, that is, the *sharpness*

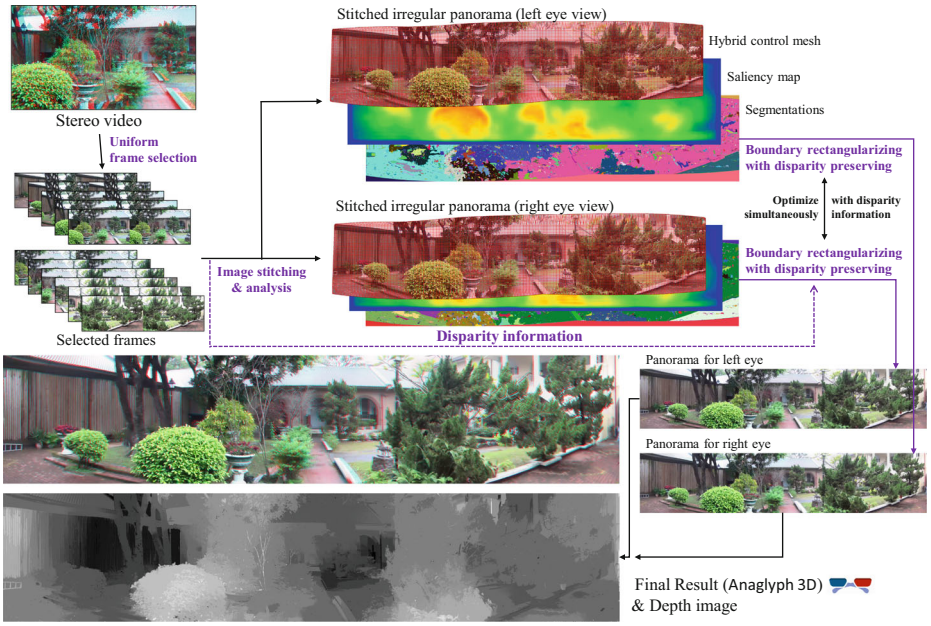

Fig. 2 An schematic diagram of the proposed approach. The final result has been rendered as a stereo image anaglyphed for red (left eye) and cyan (right eye) filters and a monochrome depth image

of the selected frames, *spatial smoothness of the adjacent selected frames*, and *spatial coverage of the selected frames*. The relative position and overlapping ratio between two adjacent frames should be also considered. However, in our study, the user will take the panoramic view for the purpose of shooting, so the movie will be slow and relatively stable. Therefore, we just select these frames uniformly with the first and last frame of stereoscopic input video. In our study, the sampling interval is 60 frames, the number of selected frames would be dependent on the length of the input. After the frame selection, we stitch these frames in the left and right videos separately into two initial panoramic images by applying the image stitching algorithm [4].

3.2 Segmentation and saliency detection

A panorama image is often composed of architectural objects or some landscape. Moreover, there may be some important and some less important objects. For this reason, similar to the method [16], we segment an image into different object patches by using the segmentation method [9] and determine the saliency by incorporating saliency detection [11] to judge whether a patch is important or not. Then, a set of patches $\mathbf{O} = \{o_1, ..., o_{n_o}\}$ and its corresponding saliency values $\mathbf{S} = \{s_1, ..., s_{n_o}\}$ are generated for warping, where n_o represents the number of patches.

3.3 Image warping energy terms

The hybrid mesh, segmentation patches and saliency values are obtained in the previous steps, the energy terms based on our warping bounding box and other preservation constraints are described as follows.

Shape deformation constraint In order to preserve the shape of the high-significance patches, the "shape deformation" energy term is used. We randomly choose a representative edge of each patch o_i to maintain the geometric relationship of all edges in each patch. Whether the representative edge is an edge of triangle mesh or an edge of quad mesh does not affect the result in any way. Hence, every edge of each patch has a relative scale and rotation relationship with their corresponding representative edge. Using this relationship between the representative edge and the other edges in each patch, the shape deformation term is formulated as,

$$E_{Sd} = \sum_{i=1}^{n_o} s_i \times \sum_{b_j \in \mathbf{B}(o_i)} \|\tilde{b}_j - \mathbf{T}_{ij}\tilde{r}_i\|^2, \tag{1}$$

where s_i is the saliency value of a patch o_i, and its range is from 0.1 to 1. $\tilde{b}_j$ and $\tilde{r}_i$ are the deformed edge and the deformedly representative edge of patch o_i, respectively. $\mathbf{T}_{ij}$ is the geometric relationship between b_j and r_i. $\mathbf{B}(o_i)$ is a set of edges which belong to the i^{th} patch. By using this energy term, we can effectively preserve the shape of important patches in the panorama image.

Grid orientation constraint As described in [16], using a triangle mesh as a control mesh in warping may have the problem of inconsistency in triangle orientations. Preserving grid orientation can avoid skew phenomenon [12, 14]. However, the boundary of stitched panorama is irregular and hard to use quad mesh to cover all regions directly. Therefore, we design a hybrid mesh to avoid this situation. In most of the regions of our panorama image, quad faces are used. In the remaining regions, triangle faces are used.

In a quad mesh, the orientation energy term of quad faces is used to keep object direction. This orientation energy term of quad faces is defined as,

$$\begin{aligned} E_{Or} = \sum_{f \in \mathbf{F}} (&\|\tilde{v}_{a_y} - \tilde{v}_{b_y}\|^2 + \|\tilde{v}_{d_y} - \tilde{v}_{c_y}\|^2 \\ &+ \|\tilde{v}_{a_x} - \tilde{v}_{d_x}\|^2 + \|\tilde{v}_{b_x} - \tilde{v}_{c_x}\|^2). \end{aligned} \tag{2}$$

Each quad has four points v_a, v_b, v_c, v_d, and this energy term is designed to avoid skew phenomenon of the quad faces after rectangularizing the panorama. Furthermore, we need to consider the joint of the quad mesh and the triangle mesh. Here, the Laplacian coordinate concept [23] is adopted. Among all junction points of a triangle mesh and quad mesh, we calculate a vector between the junction point and the mean position of its neighbors. By preserving the direction and length of this vector, we can further enhance the grid orientation of the control mesh. Then, the energy term E_{Or} has been reformulated as,

$$L(v_i) = v_i - \frac{1}{deg(v_i)} \times \sum adj(v_i), \tag{3}$$

$$E_{Or} = \sum_{i \in \mathbf{U}} \|\tilde{v}_i - \frac{\sum adj(\tilde{v}_i)}{deg(v_i)} - L(v_i)\|^2, \tag{4}$$

where $\mathbf{U}$ is the point set between quad and triangle meshes, $adj(v_i)$ is the position of a neighboring vertex of a junction point, and $deg(v_i)$ is the number of the neighbors of a junction point.

Boundary constraint This term is designed to stretch the irregular boundary of the panorama into the desired bounding box. First of all, according to the point set obtained from the contour finding algorithm [26], the user may specify four corner point on the contour and divide the contour into four point sets by its boundary position, that is, left x_L, right x_R, top y_T, and bottom y_B. Therefore, the panoramic image can be warped into the target bounding box using the energy term:

$$\begin{aligned} E_{Bc} = &\sum \|x_L\|^2 + \sum \|x_R - width\|^2 \\ &+ \sum \|y_B\|^2 + \sum \|y_T - height\|^2, \end{aligned} \tag{5}$$

where $width$ and $height$ represents to the dimensions of the bounding box.

Disparity constraint Since our input videos are stereo video, we can deduce the disparity of each pixel. In this work, we also consider how to preserve the depth information in order to provide the user with a correct spatial perception of the panorama. The previous work [18] proves that minimizing the difference between the disparity vector of the corresponding feature in the input and deformed frames could effectively provide consistent deformation in left and right frames. Therefore, a disparity preserving energy term is also introduced to preserve the depth information in this work. First, several feature points are extracted from the selected frames by using the SIFT method, and the corresponding pair (p_i^L, p_i^R) between these feature points in the left and right images are then established. The matched feature points are called source feature points. To eliminate any outliers, RANSAC [10] is applied. Based on our selected frames, we measure the disparity of these source feature point pairs as follows.

$$Disp_i = p_i^L - p_i^R, \tag{6}$$

where the suffix i represents the index of matched points in the right and left eye images of a selected frame. Next, we find the destination point pairs between the left and right irregular panoramas according to a similar idea described above. To preserve correct depth perception of input video frames, we also minimize the difference of disparity between the source and destination feature pair set. Because of the specialization of the hybrid mesh, there are three possible combinations of correspondence, that is, (quad mesh, quad mesh), (quad mesh, triangle mesh), and (triangle mesh, triangle mesh). Here, the barycentric coordinate is used to transfer destination feature points into a mesh point representation. In the three combinations of meshes, all feature points can be represented by a linear combination of the surrounding mesh points, and the abovementioned energy terms are formulated as,

$$E_{Dp} = \sum_{i=1}^{N_f} \|(f_i^L - f_i^R) - \begin{bmatrix} S_x & 0 \\ 0 & S_y \end{bmatrix} \times Disp_i\|^2, \tag{7}$$

$$f^L = \begin{cases} \sum_{m=1}^{3} b_m^L \tilde{v}_m^L, & \text{if } f^L \text{ is enclosed by triangle } (\tilde{v}_1^L, \tilde{v}_2^L, \tilde{v}_3^L) \\ \sum_{m=1}^{4} b_m^L \tilde{v}_m^L, & \text{if } f^L \text{ is enclosed by quad } (\tilde{v}_1^L, \tilde{v}_2^L, \tilde{v}_3^L, \tilde{v}_4^L), \end{cases} \tag{8}$$

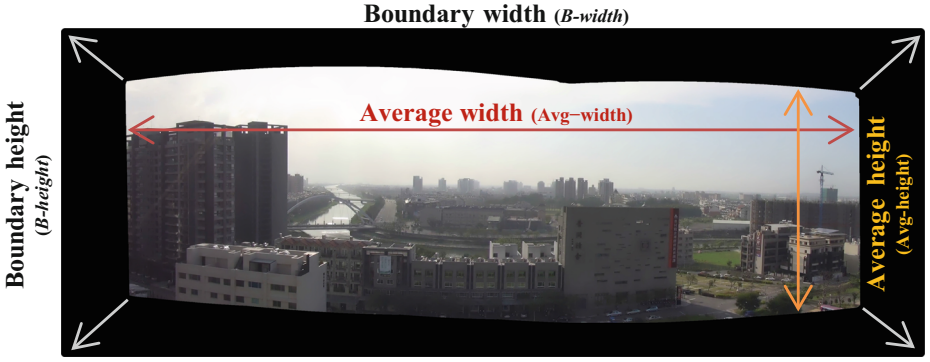

Fig. 3 Similar transformation ratio. The center region is stitched irregular panorama, and the outer boundary is representing the boundary of output regular panorama

$$f^R = \begin{cases} \sum_{m=1}^{3} b_m^R \tilde{v}_m^R, & \text{if } f^R \text{ is enclosed by triangle } (\tilde{v}_1^R, \tilde{v}_2^R, \tilde{v}_3^R) \\ \sum_{m=1}^{4} b_m^R \tilde{v}_m^R, & \text{if } f^R \text{ is enclosed by quad } (\tilde{v}_1^R, \tilde{v}_2^R, \tilde{v}_3^R, \tilde{v}_4^R), \end{cases} \tag{9}$$

where N_f denotes the total number of feature pairs. The matrix $\begin{bmatrix} S_x & 0 \\ 0 & S_y \end{bmatrix}$ represents the similarity transformation which defined as $\frac{B-width}{Avg-width}$ and $\frac{B-height}{Avg-height}$ as illustrated in Fig. 3. b_m denotes the coefficient of the barycentric coordinates associated with the vertex v_m.

By combining all the energies, the optimization for the mesh warping is formulated as:

$$E_{warping} = w_1 E_{Sd} + w_2 E_{Or} + w_3 E_{Bc} + w_4 E_{Dp}, \tag{10}$$

where E_{Sd}, E_{Or}, E_{Bc}, and E_{Dp} represent the shape deformation, grid orientation, boundary, and disparity constraints, respectively. Also, we use several weighting factors w_1, w_2, w_3, w_4 to prevent each term to dominate another. In our experiments, these weighting factors at Eq. 10 are 5, 5, 1000, 1. One of the important considerations of weighting is the strength of the constraints. The others are mainly derived from the range distribution of the energy terms and some experimental processes in our study.

Table 1 Computational performance of our system

Figure #	Resolution	# of whole frames	# of representative frames	Stitching (ms)	Rectangular -izing(ms)
4	3142×1080	346	7	131501	3142
6(a)	5185×1080	600	11	284650	7331
6(b)	3200×1080	960	17	61822	3423
7(a)	5237×1080	1186	21	206344	7490
7(b)	4936×1080	496	10	183322	7821
8(a)	5163×1080	260	6	53367	6132
8(b)	4799×1080	305	7	70213	6211
9(a)	3724x1080	276	7	12278	4620
9(b)	3847x1080	301	7	11286	3854
9(c)	2905x1080	288	7	10589	2628

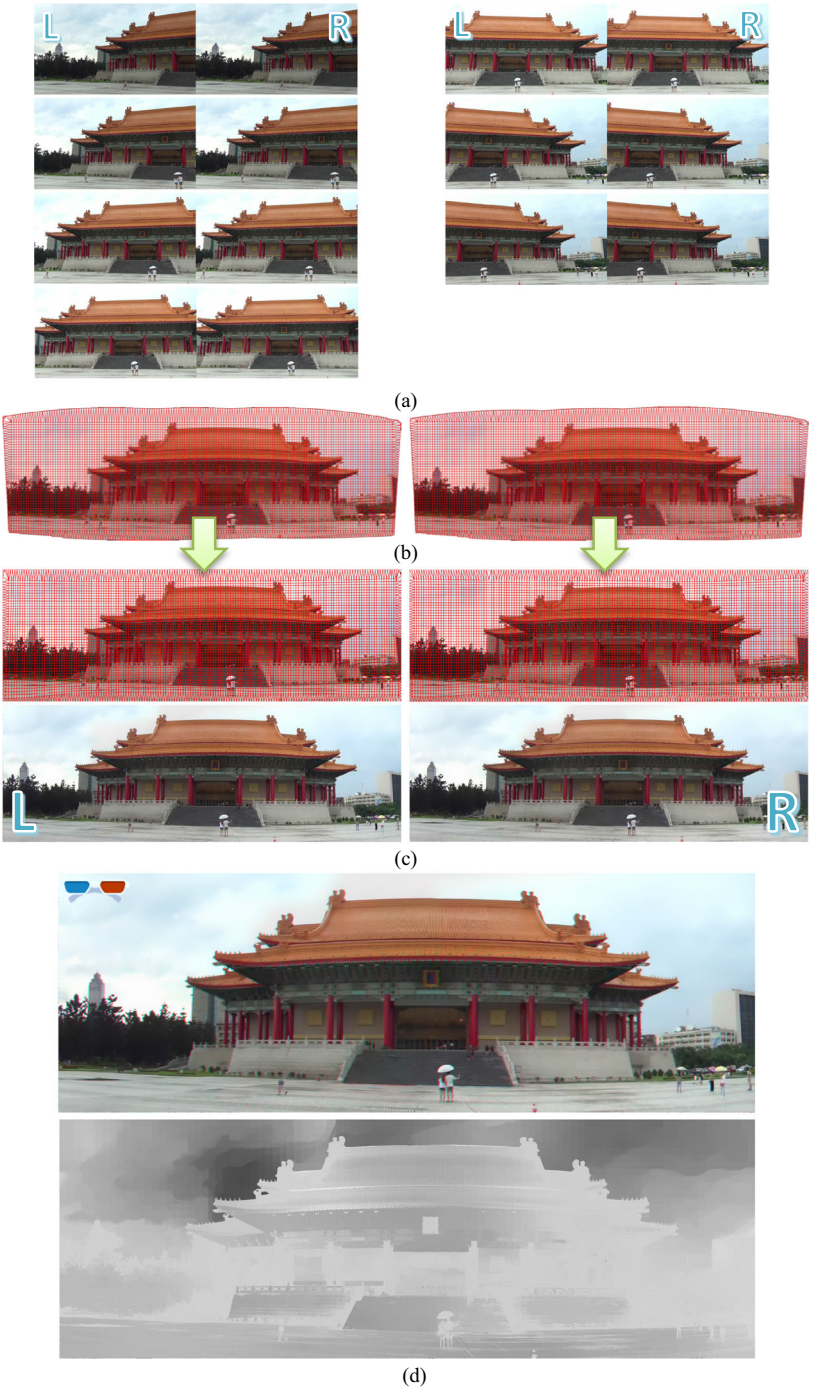

Fig. 4 **a** Selected frames of stereoscopic film **b** stitched panoramic image of left eye and right eye with hybrid meshes **c** warped panoramic image with/without hybrid meshes **d** the generated stereoscopic panoramic image and its depth image

4 Experimental results and discussion

The experimental results are generated using a PC with 3.0 GHz CPU and 4 GB memory. The computational performance of the proposed methods is shown in Table 1. On average, for an input video in 3480x1080 resolution, the computation time for image stitching and panorama rectangularizing is few minutes and few seconds, respectively. The selected frames, stitched panoramic image, and the generated stereoscopic panoramic image with its depth map are shown in Fig. 4. The software DMAG5 [5] and DMAG9b [6] generated

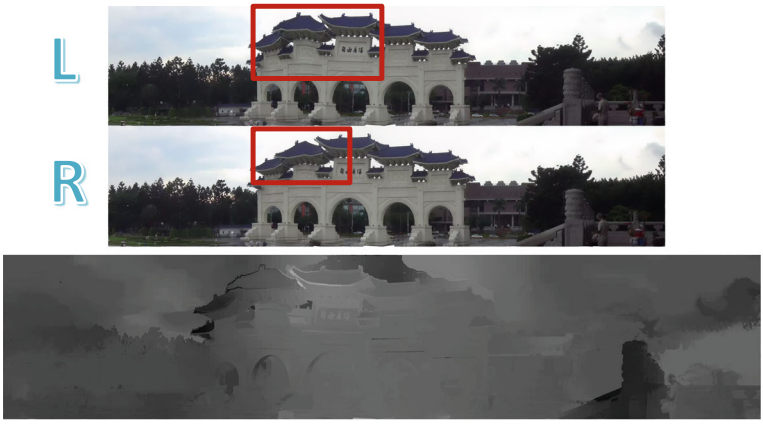

(a)

(b)

Fig. 5 Examples of adopting state-of-art rectangling approach [13] to rectangle left and right panoramic images without considering depth information. The rectangularied results are inconsistent between left and right panoramas. The reconstructed depth images by DMAG5 [5] are also troublesome

all depth image shown on this paper and provided on this blog [7]. This software is an implementation of several state-of-art research works including but not limited to [29],[22], and [3].

To demonstrate the feasibility of the disparity constraint, rectangularizing with and without disparity term is conducted. We adopt a state-of-art rectangling approach [13] to rectangle left and right panoramic images via warping directly and compose it into one

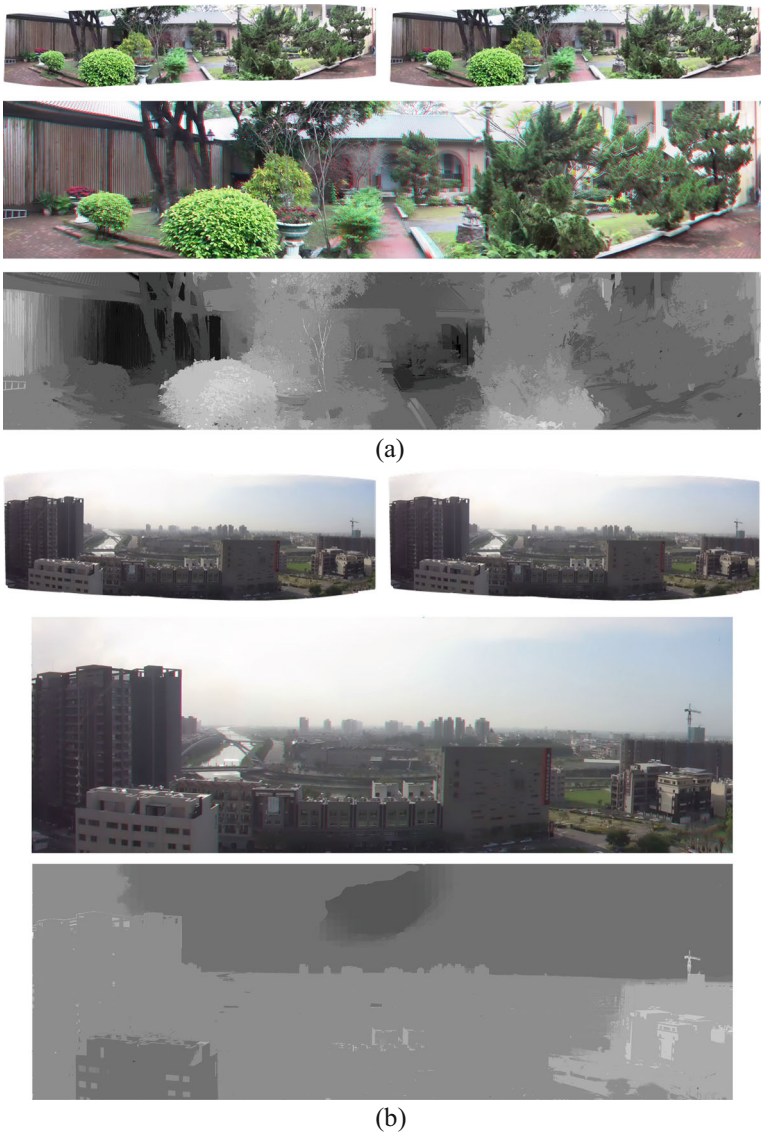

Fig. 6 Results (p6a and p6b) created by our system

stereoscopic panoramic image. The results are shown in Fig. 5. The shapes of the salient patches are still preserved. Although the distortion of the left and right panoramic image may be minimized to an acceptable result. The warping of left and right image may not have consistency. Without careful consideration of disparity preservation, the pixel disparities cannot be maintained as shown in Fig. 5. By contrast, when the disparity and shape preservation energy terms are used in the boundary rectangularizing, both the spatial shapes and disparity of salient patches are preserved, as shown in Figs. 6, 7 and 8 show other stereoscopic panoramic results generated by our system. Figure 9 showss more results with hybrid mesh which generated by our system, too. Also, quantitative analysis is conducted to evaluate the disparity preservation of our results. Here, the quality of pixel disparities in

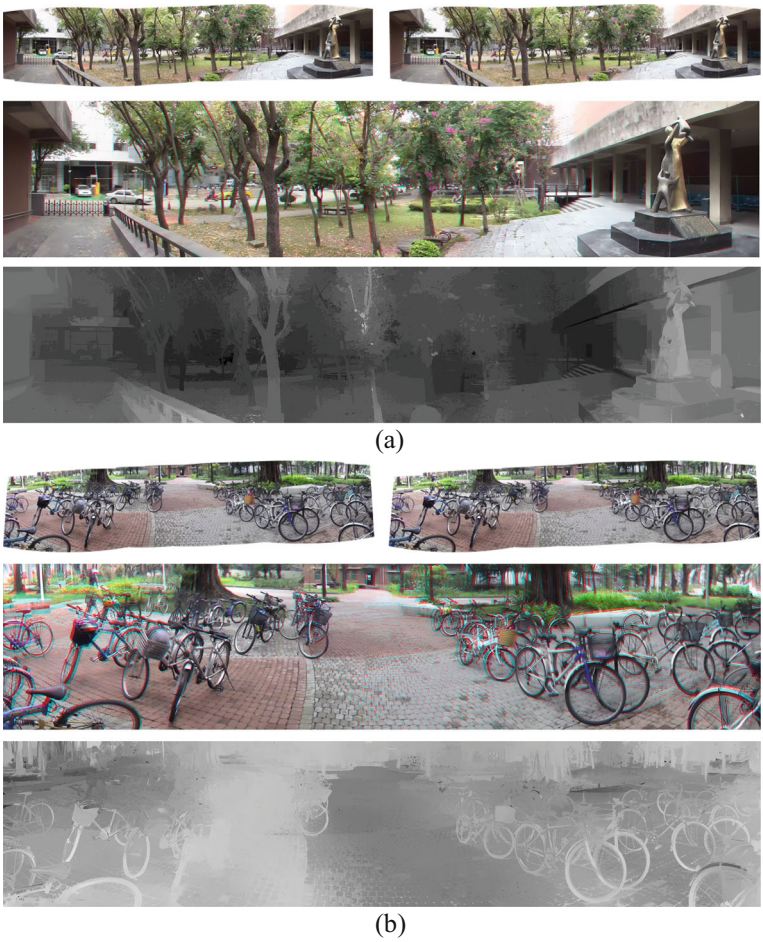

Fig. 7 More results (p7a and p7b) created by our system

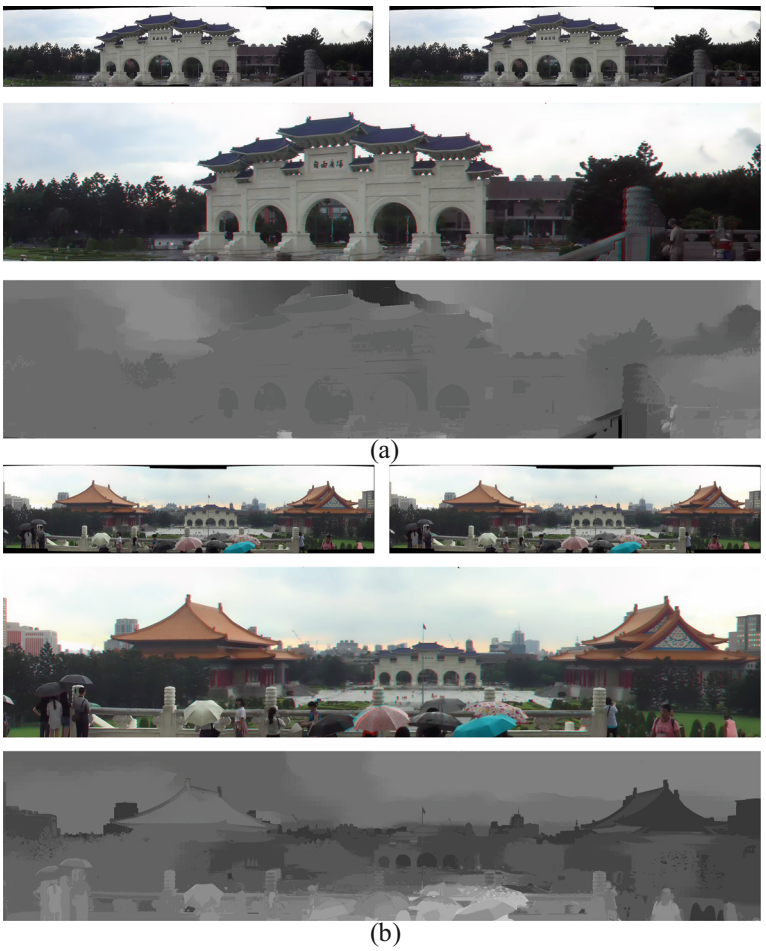

Fig. 8 More results (p8a and p8b) created by our system

the generated stereoscopic panoramas is defined as measuring the difference between the disparities of source feature pairs and that of destination feature pairs, given by,

$$D_{err} = \frac{1}{N_f} \sum_{i=1}^{N_f} \|(S_i^L - S_i^R) - (d_i^L - d_i^R)\|^2, \tag{11}$$

where $(S_i^L - S_i^R)$ denotes to i^{th} source feature pair in a representative frame, and $(d_i^L - d_i^R)$ denotes the i^{th} destination feature pair in irregular or rectangularized stereoscopic panoramic result. N_f represents the total number of feature pairs. In an optimal case, the difference D_{err} of these vectors is minimized. The comparison results are shown in Table 2, and from this table it can be seen that our method is significantly better than irregular stitching. Also, the result of rectangularized stereoscopic panorama without depth

Fig. 9 More results (p9a, p9b, p9c) with hybrid mesh created by our system

Table 2 Quantitative analysis of disparity preservation

Figure #	Resolution Disparity of	Disparity of method A	Disparity of method B	method C
4	3142×1080	2.762	0.885	2.249
6(a)	5185×1080	29.370	1.619	8.365
6(b)	3200×1080	4.234	1.057	6.420
7(a)	5237×1080	5.764	1.040	7.303
7(b)	4936×1080	4.465	2.682	8.761
8(a)	5163×1080	2.164	0.851	10.217
8(b)	4799×1080	2.251	0.939	5.954
9(a)	3724x1080	3.614	1.187	10.538
9(b)	3847x1080	4.774	1.429	77.372
9(c)	2905x1080	3.527	1.769	14.127

Methods A denotes irregular stitching, method B denote rectangularized stereoscopic panorama generated by proposed method, method C denote rectangularied it with method [13] and compose left and right image directly

information also be tested and the quantitative analysis shows that the disparity of original stitching has been lost.

5 Conclusion and future work

In this paper, a practical system to generate a stereoscopic panorama from a stereoscopic video is proposed. Our system effectively preserved the disparity on the rectangularizing step and stereoscopic information well. The results, as mentioned above, show our disparity-aware panorama rectangularizing step is reliable for handling different cases.

Nevertheless, there are some limitations of our system. First of all, image stitching with uniformly selected frames has its limitation. The moving speed of 3D camera should not be too fast. The limitation of the speed and stability may vary significantly according to different stitching methods, and this part is not the focus of our research in this paper. It can also be changed to other implementation issues easily. Besides, when image stitching is confronted with the parallax problem and fast action foreground objects, it may suffer from a ghost effect. Parallax problems appear when video captures the same content from different viewpoints. Zhang et al [31] solve this problem elegantly by using homography and warping technique. Besides, in some cases, the effectiveness of disparity preserving may depend on the uniform distribution of feature points. Therefore, several stereoscopic image stiitching techniques [28, 32] may be consider as a good start to explore this problem from different aspects.

For future work, we can address the parallax problem by adapting their parallax tolerant image stitching method. Second, our method can handle the small variation of depth information. If the video contents have a significant disparity variation, it may lead to an unpleasing panorama result. Considering the disparity issue, further work includes extending the range of depth and adapting to complex camera motion to provide users a more exciting result with visually plausible depth perception.

Acknowledgements We thank the anonymous reviewers for valuable comments and Cheng-Yue Qiu and Yun-Chen Lin for taking some exprimental videos and preproessing results. This work was supported by Ministry of Science and Technology under no. 108-2221-E-155-033-MY2, 108-2221-E-019-038-MY2, 108-2221-E-006-038-MY3 and 107-2221-E-006-196-MY3.

References

1. Agarwala A, Zheng KC, Pal C, Agrawala M, Cohen M, Curless B, Salesin D, Szeliski R (2005) Panoramic video textures. ACM Trans Graph 24(3):821–827
2. Barnes C, Shechtman E, Finkelstein A, Goldman DB (2009) Patchmatch: a randomized correspondence algorithm for structural image editing. ACM Trans Graph 28(3):24:1–24:11
3. Barron JT, Poole B (2016) The fast bilateral solver. In: European conference on computer vision. Springer, pp 617–632
4. Brown M, Lowe DG (2007) Automatic panoramic image stitching using invariant features. Int J Comput Vision 74(1):59–73
5. Capeto U (2014) Depth map automatic generator 5 (dmag5). http://3dstereophoto.blogspot.com/2014/05/depth-map-automatic-generator-5-dmag5.html. Accessed 2019 May 10
6. Capeto U (2015) Depth map automatic generator 9 (dmag9). http://3dstereophoto.blogspot.com/2015/12/depth-map-automatic-generator-9-dmag9.html. Accessed 2019 May 10
7. Capeto U (2019) 3d stereoscopic photography, 3d software. http://3dstereophoto.blogspot.com/p/software.html. Accessed 2019 May 10
8. Chang CH, Liang CK, Chuang YY (2011) Content-aware display adaptation and interactive editing for stereoscopic images. IEEE Trans Multi 13(4):589–601
9. Felzenszwalb PF, Huttenlocher DP (2004) Efficient graph-based image segmentation. Int J Comput Vision 59(2):167–181
10. Fischler MA, Bolles RC (1981) Random sample consensus: a paradigm for model fitting with applications to image analysis and automated cartography. Commun of the ACM 24(6):381–395
11. Goferman S, Zelnik-Manor L, Tal A (2012) Context-aware saliency detection. IEEE Trans Pattern Anal Mach Intell 34(10):1915–1926
12. Guo Y, Liu F, Shi J, Zhou ZH, Gleicher M (2009) Image retargeting using mesh parametrization. IEEE Trans Multi 11(5):856–867
13. He K, Chang H, Sun J (2013) Rectangling panoramic images via warping. ACM Trans Graph 32(4):79:1–79:10
14. Jin Y, Liu L, Wu Q (2010) Nonhomogeneous scaling optimization for realtime image resizing. Vis Comput 26(6-8):769–778
15. Kopf J, Kienzle W, Drucker S, Kang SB (2012) Quality prediction for image completion. ACM Trans Graph 31(6):131:1–131:8
16. Lin SS, Yeh IC, Lin CH, Lee TY (2013) Patch-based image warping for content-aware retargeting. IEEE Trans Multi 15(2):359–368
17. Lin SS, Lin CH, Chang SH, Lee TY (2014) Object-coherence warping for stereoscopic image retargeting. IEEE Trans Circuits Syst Video Techn 24(5):759–768
18. Lin SS, Lin CH, Kuo YH, Lee TY (2016) Consistent volumetric warping using floating boundaries for stereoscopic video retargeting. IEEE Trans Circuits Syst Video Techn 26(5):801–813
19. Liu F, Hu YH, Gleicher ML (2008) Discovering panoramas in web videos. In: Proceedings of the 16th ACM international conference on multimedia, pp 329–338
20. Niu Y, Feng WC, Liu F (2012) Enabling warping on stereoscopic images. ACM Trans Graph 31(6):183:1–183:7
21. Oettermann S (1997) The panorama: history of a mass medium, 1st edn. Zone Books
22. Rhemann C, Rother C (2012) Fast cost-volume filtering for visual correspondence and beyond. In: CVPR
23. Shewchuk JR (1996) Triangle: engineering a 2d quality mesh generator and delaunay triangulator. In: Selected papers from the workshop on applied computational geormetry, towards geometric engineering, pp 203–222
24. Shum HY, Szeliski R (2000) Systems and experiment paper: construction of panoramic image mosaics with global and local alignment. Int J Comput Vision 36(2):101–130
25. Sorkine O, Cohen-Or D, Lipman Y, Alexa M, Rössl C, Seidel HP (2004) Laplacian surface editing. In: Proceedings of the 2004 eurographics/ACM SIGGRAPH symposium on geometry processing, pp 175–184

26. Suzuki S, Abe K (1985) Topological structural analysis of digitized binary images by border following. Comput Vis Graph Image Process 30(1):32–46
27. Yan T, Huang Z, Lau RWH, Xu Y (2013) Seamless stitching of stereo images for generating infinite panoramas. In: Proceedings of the 19th ACM symposium on virtual reality software and technology, pp 251–258
28. Yan W, Hou C, Lei J, Fang Y, Gu Z, Ling N (2017) Stereoscopic image stitching based on a hybrid warping model. IEEE Transactions on Circuits and Systems for Video Technology 27(9):1934–1946
29. Yoon KJ, Kweon IS (2006) Adaptive support-weight approach for correspondence search. IEEE transactions on pattern analysis and machine intelligence (4): 650–656
30. Zaragoza J, Chin TJ, Brown MS, Suter D (2013) As-projective-as-possible image stitching with moving dlt. In: Proceedings of the 2013 IEEE conference on computer vision and pattern recognition, pp 2339–2346
31. Zhang F, Liu F (2014) Parallax-tolerant image stitching. In: Proceedings of the 2014 IEEE conference on computer vision and pattern recognition, pp 3262–3269
32. Zhang F, Liu F (2015) Casual stereoscopic panorama stitching. In: 2015 IEEE conference on computer vision and pattern recognition (CVPR), pp 2002–2010